JACS
JOURNAL OF THE AMERICAN CHEMICAL SOCIETY
Article
pubs.acs.org/JACS

Polymorph-Specific Kinetics and Thermodynamics of β-Amyloid Fibril Growth

Wei Qiang, Kevin Kelley,[#] and Robert Tycko*

Laboratory of Chemical Physics, National Institute of Diabetes and Digestive and Kidney Diseases, National Institutes of Health, Bethesda, Maryland 20892-0520, United States

Supporting Information

ABSTRACT: Amyloid fibrils formed by the 40-residue β-amyloid peptide ($A\beta_{1-40}$) are highly polymorphic, with molecular structures that depend on the details of growth conditions. Underlying differences in physical properties are not well understood. Here, we investigate differences in growth kinetics and thermodynamic stabilities of two $A\beta_{1-40}$ fibril polymorphs for which detailed structural models are available from solid-state nuclear magnetic resonance (NMR) studies. Rates of seeded fibril elongation in the presence of excess soluble $A\beta_{1-40}$ and shrinkage in the absence of soluble $A\beta_{1-40}$ are determined with atomic force microscopy (AFM). From these rates, we derive polymorph-specific values for the soluble $A\beta_{1-40}$ concentration at quasi-equilibrium, from which relative stabilities can be derived. The AFM results are supported by direct measurements by ultraviolet absorbance, using a novel dialysis system to establish quasi-equilibrium. At 24 °C, the two polymorphs have significantly different elongation and shrinkage kinetics but similar thermodynamic stabilities. At 37 °C, differences in kinetics are reduced, and thermodynamic stabilities are increased significantly. Fibril length distributions in AFM images provide support for an intermittent growth model, in which fibrils switch randomly between an "on" state (capable of elongation) and an "off" state (incapable of elongation). We also monitor interconversion between polymorphs at 24 °C by solid-state NMR, showing that the two-fold symmetric "agitated" ($\mathcal{A}$) polymorph is more stable than the three-fold symmetric "quiescent" ($\mathcal{Q}$) polymorph. Finally, we show that the two polymorphs have significantly different rates of fragmentation in the presence of shear forces, a difference that helps explain the observed predominance of the $\mathcal{A}$ structure when fibrils are grown in agitated solutions.

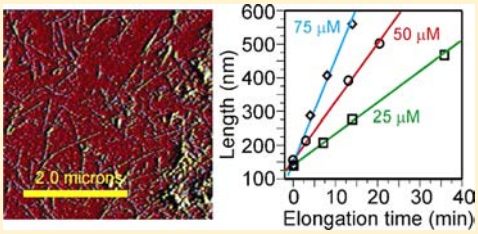

INTRODUCTION

Alzheimer's disease (AD) is characterized by the formation of neurotoxic β-amyloid (Aβ) plaques in brain tissue. The amyloid deposits contain Aβ fibrils with primarily 40-residue ($A\beta_{1-40}$) and 42-residue ($A\beta_{1-42}$) sequences. In vitro studies have shown that Aβ fibrils formed under various experimental conditions possess distinct molecular structures.[1−7] Although a variety of $A\beta_{1-40}$ and $A\beta_{1-42}$ fibril structures have been characterized in varying levels of detail,[3,4,8−19] kinetic and thermodynamic differences among these structures that may influence the observed dependence of molecular structure on growth conditions are not fully characterized. In particular, our laboratory has shown that the predominant $A\beta_{1-40}$ fibril morphology that develops de novo (i.e., in the absence of pre-existing fibril seeds) is strongly affected by the presence or absence of agitation of the $A\beta_{1-40}$ solution.[2] At 24 °C, pH 7.4, and low ionic strength, the majority of fibrils that form in a quiescent solution are single filaments with an apparent periodic twist about the fibril growth axis, as in Figure 1A. Under the same buffer conditions, but with agitation of the solution, the majority of fibrils occur as bundles of multiple filaments, as in Figure 1B. "Quiescent" ($\mathcal{Q}$) and "agitated" ($\mathcal{A}$) $A\beta_{1-40}$ fibrils have distinct ^{13}C chemical shifts in solid-state nuclear magnetic resonance (NMR) spectra[2−4] and distinct mass-per-length values,[2,5,6,20] in addition to their distinct appearances in transmission electron microscope (TEM) images. According to detailed structural models developed from solid-state NMR and electron microscopy data, $\mathcal{Q}$ fibrils have approximate three-fold rotational symmetry about the fibril growth axis,[4] while protofilaments within $\mathcal{A}$ fibrils have two-fold rotational symmetry.[3] It has been unclear whether $\mathcal{Q}$ and $\mathcal{A}$ fibrils have different thermodynamic stabilities or different growth kinetics, and it has been unclear why the presence or absence of gentle agitation has such a profound structural effect.

As demonstrated by others,[7,21−25] thermodynamic stabilities of amyloid fibrils, including dependences of thermodynamic stabilities on amino acid substitutions and polymorphism, can be assessed from direct measurements of the concentration of peptide monomers that are in quasi-equilibrium with the fibrils. An alternative approach is to measure the elongation rates k_e of fibrils in the presence of excess monomers and the shrinkage rates k_s in the absence of monomers.[26−30] Assuming that fibrils elongate or shrink by addition or subtraction of monomers, and with other reasonable assumptions (see Discussion section), the average fibril length L is expected to follow an equation of the form

Received: December 7, 2012
Published: April 22, 2013

   dx.doi.org/10.1021/ja311963f | J. Am. Chem. Soc. 2013, 135, 6860−6871

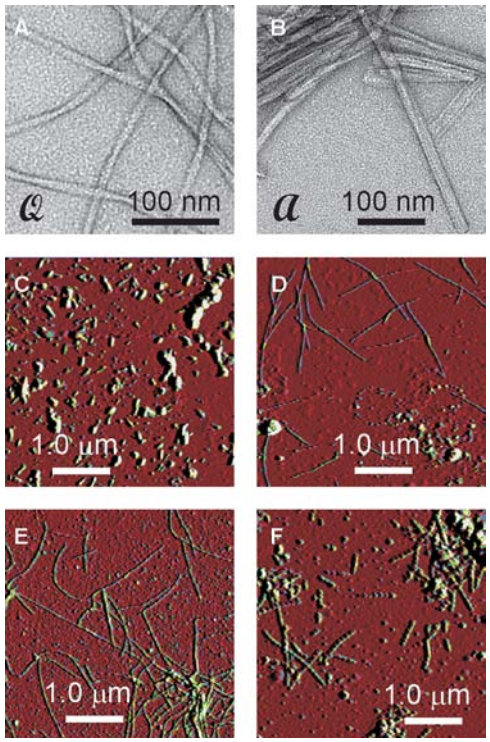

Figure 1. (A,B) Negatively stained TEM images of "quiescent" and "agitated" Aβ_{1-40} fibrils (called $\mathcal{Q}$ and $\mathcal{A}$ fibrils), showing their distinct morphologies. These fibrils resulted from seeded growth at 24 °C, using 50 μM initial monomer concentrations. (C,D) Representative AFM images of $\mathcal{Q}$ fibrils from elongation measurements after 0 and 20 min incubation, respectively. Measurements were done at 24 °C with 50 μM soluble Aβ_{1-40} concentration. (E,F) Representative AFM images of $\mathcal{Q}$ fibrils from shrinkage measurements at 24 °C after 2 and 46 h incubation, respectively. Vertical scales represent AFM feedback error signals, not height.

$$\frac{dL}{dt} = k_e M - k_s \quad (1)$$

where M is the time-dependent monomer concentration. Note that k_e can have units of nm/s·μM, while k_s can have units of nm/s. At quasi-equilibrium ($dL/dt = 0$), the monomer concentration is $M_{QE} = k_s/k_e$. This indirect approach to assessment of thermodynamic stability has several potential advantages, including insensitivity to chemical impurities, no requirement for separation of fibrils from monomers, no requirement that a quasi-equilibrium state be reached, and ability to measure small values of M_{QE}. This approach also yields interesting kinetic parameters.

In this paper, we describe the use of atomic force microscopy (AFM) to measure the time dependences of Aβ_{1-40} fibril length distributions in the presence of various Aβ_{1-40} monomer concentrations, allowing k_s and k_e to be determined. We report measurements for $\mathcal{Q}$ and $\mathcal{A}$ fibrils, allowing the thermodynamic stabilities and kinetic properties of the two Aβ_{1-40} fibril polymorphs to be compared. The time dependences of fibril length distributions provide evidence for intermittent growth of individual fibrils,[30−32] possibly due to structural transitions of fibril ends between "on" and "off" states. We show that values of M_{QE} determined from the AFM measurements are in good agreement with direct measurements of soluble Aβ_{1-40} by ultraviolet (UV) absorbance, using a dialysis technique that separates soluble species from fibrils without uncertainties inherent in separation by centrifugation. We find that $\mathcal{Q}$ and $\mathcal{A}$ fibrils have similar thermodynamic stabilities (i.e., similar values of M_{QE}) despite their different molecular structures, but significantly different elongation and shrinkage kinetics. At 24 °C under our buffer conditions, M_{QE} values determined by AFM and by UV ($M_{QE,AFM}$ and $M_{QE,UV}$) suggest that $\mathcal{A}$ fibrils are slightly more stable than $\mathcal{Q}$ fibrils, a finding that is supported by direct measurements of structural interconversion using solid-state NMR. Finally, we discuss factors that may contribute to the observed dependence of fibril structure on growth conditions and show that differences in susceptibility to fragmentation under shear forces are an important factor.

In the preceding introduction and in the following sections, we use the term "quasi-equilibrium" to describe a state in which fibrils with a particular morphology and molecular structure are effectively in a steady state with soluble Aβ_{1-40} (monomer and possibly small oligomers). Such a state is not necessarily a true equilibrium state, because this particular fibril structure may not be the most stable fibril structure. In principle, the quasi-equilibrium state could evolve slowly toward a state in which the fibrils have converted to a more stable structure. However, as shown below, such evolution is practically unobservable in the absence of seeds of the more stable structure, because values of M_{QE} are so small that nucleation of the more stable structure is inefficient and because different fibril polymorphs do not interconvert by internal structural rearrangements. The existence of quasi-equilibrium states for individual fibril polymorphs is a prerequisite for studies of the type described below.

MATERIALS AND METHODS

Fibril Elongation Measurements. Aβ_{1-40} was prepared by solid-phase peptide synthesis, using an Applied Biosystems 433A automated synthesizer, and purified by high-performance liquid chromatography (HPLC), using a Beckman-Coulter model 125P solvent pump module and model 168 detector, a Zorbax 300SB-C3 column (Agilent), and a H_2O/acetonitrile gradient with 1.0% trifluoroacetic acid. Purity was assessed by electrospray ionization mass spectrometry (1100 MSD, Hewlett-Packard) and found to be >95%. After purification, the peptide was lyophilized and stored at −20 °C. $\mathcal{Q}$ fibrils were prepared by seeded growth, using one of the solid-state NMR samples described by Paravastu et al.[4] as the original source of seeds. A portion of the NMR sample (~0.5 mg of fibrils) was added to 1 mL of incubation buffer (10 mM phosphate, pH 7.4, 0.01% NaN_3), sonicated to break the fibrils into short fragments (Branson model S-250A sonifier with tapered 1/8″ microtip horn, lowest power, 10% duty factor, 2 min), and diluted to 5 mL in incubation buffer in a vertical 20 mL tube. Purified, lyophilized Aβ_{1-40} was dissolved in dimethyl sulfoxide (DMSO) to a concentration of 8 mM. An aliquot of DMSO-solubilized Aβ_{1-40} was then added to the 5 mL seed solution to produce a 100 μM Aβ_{1-40} concentration (not including seeds) and immediately mixed by vortexing. After 24 h of quiescent incubation at ambient temperature, the solution gelled due to growth and entanglement of fibrils. The gel was readily disrupted by vortexing. The predominant fibril morphology was confirmed by TEM to match the "twisted" morphology described by Paravastu et al.[4] An aliquot of these fibrils was then used as seeds for a second generation of seeded growth. Fibrils from the second generation were used in experiments described below.

$\mathcal{A}$ fibrils were prepared by diluting DMSO-solubilized Aβ_{1-40} to 230 μM in incubation buffer. A 5 mL volume of the Aβ_{1-40} solution was incubated in a 20 mL tube, lying horizontally on an orbital platform shaker (VWR model DS-500E). The agitation frequency (roughly 1 Hz) was adjusted to produce a "sloshing" motion of the solution along the length of the tube. A visible precipitate of Aβ_{1-40} fibrils developed within 12 h. The predominant fibril morphology was

dx.doi.org/10.1021/ja311963f | J. Am. Chem. Soc. 2013, 135, 6860−6871

confirmed by TEM to match the "striated ribbon" morphology described previously by Petkova et al.[2,3] These $\mathcal{A}$ fibrils were then used as seeds for growth of a second generation of $\mathcal{A}$ fibrils, at 100 μM Aβ_{1-40} concentration. Fibrils from the second generation were used in experiments described below.

For fibril elongation measurements by AFM at ambient temperature (24 °C), a 25 μL aliquot of fibril solution (either $\mathcal{A}$ or $\mathcal{Q}$) was added to 1.0 mL of incubation buffer. For measurements at 37 °C, 6.25 μL of fibril solution was added to 0.5 mL of incubation buffer. The diluted fibril solution was then sonicated for 2 min on an ice bath and was kept at 24 or 37 °C for at least 10 min for temperature equilibration. DMSO-solubilized Aβ_{1-40} was then added to reach the desired final concentrations, i.e., 25, 50, and 75 μM for measurements at 24 °C and 13, 27, and 40 μM for measurements at 37 °C. Fibrils were allowed to elongate, and 20 μL aliquots were taken at various time points for AFM imaging.

Note that the precise values of fibril seed concentrations and seed lengths do not affect the experiments described below, because lengths of individual fibrils (rather than total fibril mass) are measured by AFM. Final DMSO concentrations in all experiments were <2% by volume.

Fibril Shrinkage Measurements. Fibril shrinkage was measured by AFM on freshly prepared fibrils under dialysis conditions, using the apparatus depicted in Figure S1. To prepare the fibrils, 0.5 mg of DMSO-solubilized Aβ_{1-40} was added to a solution of seeds in incubation buffer to produce a 50 μM Aβ_{1-40} concentration (not including the seeds). Fibril growth was then allowed to proceed for 3 h at 24 °C or 1 h at 37 °C. Fibrils were then pelleted by ultracentrifugation for 1 h at 432 000 × g and 4 °C (Beckman-Coulter Optima ultracentrifuge, TLA100.2 rotor). The residual Aβ_{1-40} concentration in the supernatant was determined by analytical HPLC, as described below, to ensure that fibril growth was essentially complete. The pellet was resuspended in 1 mL of incubation buffer, thoroughly mixed, and diluted to 25 mL in incubation buffer. A 1 mL aliquot of the diluted solution, containing ∼0.02 mg of fibrils, was transferred to a dialysis tube (Spectrum Laboratories Float-A-Lyzer G2, 300 kDa MWCO, 1 mL volume) and dialyzed against 30 mL of incubation buffer in a 50 mL Falcon tube. Magnetic stir bars were placed both inside the dialysis tube and in the buffer reservoir. The entire dialysis system was flushed with a gentle N_2 flow to prevent oxidation of Aβ_{1-40}. Importantly, the N_2 flow was low enough that there was negligible evaporation of total buffer volume during the dialysis period. Aliquots of the solution inside the dialysis tube were taken at various time points for AFM imaging.

The stir bar within the dialysis tube prevented fibrils from settling to the bottom of the tube during shrinkage experiments. The stir bar rotated at roughly 0.3 Hz. At this low stirring rate, fragmentation of fibrils due to shear forces was negligible. For measurements at 37 °C, the entire dialysis system was heated and thermally insulated as shown in Figure S1. Temperature was stabilized at 37° ± 3 °C for the duration of these measurements, as monitored by a thermometer in the buffer reservoir.

AFM Measurements. For each image, a 20 μL aliquot of fibril solution was deposited on a freshly cleaved, dry mica surface. The solution was adsorbed for 1 min before blotting by tissue paper. The mica surface was then washed once with 500 μL of deionized water and dried under a gentle N_2 flow. For aliquots containing short fibrils (first time point in elongation experiments), one additional washing step was required in order to remove buffer salts from the mica surface that otherwise interfered with fibril length measurements. AFM images were recorded in tapping mode using a Veeco MultiMode instrument and Nanoscope IV controller, equipped with Veeco DMASP tips. The tip oscillation frequency was typically 250 kHz, with a drive amplitude of 100−150 mV and a detector set point of ∼0.6 V. Images typically contained 512 × 512 points in a 8.0 × 8.0 μm area, scanned at 1.0 μm/s rate. Height, feedback error signal, and phase images were recorded simultaneously. Error signal images were used for fibril length measurements and are shown in the figures (except where indicated), because these images did not require baseline subtraction.

To measure fibril length distributions, images from the AFM software were imported into ImageJ.[33] All objects in an image with fibrillar appearance (i.e., with obvious asymmetry and with the expected apparent width and height) that were separated from other fibrils and that were fully contained within the image field were selected for measurements. Lengths were measured manually with the standard ImageJ freehand line selection tool. Lengths of curved fibrils were obtained by summing the lengths of straight sections.

Measurement of M_{QE} by UV Absorbance. Values of M_{QE}, representing soluble Aβ_{1-40} concentration at quasi-equilibrium, were also measured directly by UV absorbance in an analytical HPLC system. For these measurements, fibrils were prepared as for fibril shrinkage experiments, and the same dialysis system was used. After ultracentrifugation, fibril pellets were resuspended in 2 mL of incubation buffer and mixed thoroughly. A 1 mL aliquot, containing ∼0.25 mg of fibrils, was transferred to a dialysis tube without further dilution and dialyzed against 30 mL of incubation buffer for ∼4 days. The dialysis system was flushed continuously with a gentle N_2 flow to prevent oxidation of Aβ_{1-40}. Aliquots of 0.5 mL were taken from the buffer reservoir and subjected to analytical HPLC measurements at 0, 24, 48, 72, and 96 h after the beginning of the dialysis process. Under these conditions, we found that quasi-equilibrium was established by 72 h. HPLC measurements (Beckman-Coulter model 125P solvent pump module, model 168 detector, Vydac 218TP104 reverse-phase C18 column) used a linear H_2O/acetonitrile gradient (from 10% to 90% acetonitrile in 40 min) with 0.1% trifluouroacetic acid. The Aβ_{1-40} peak eluted at ∼16 min, as confirmed using matrix-assisted laser-desorption-ionization time-of-flight mass spectrometry (Axima-CFR, Shimadzu). At 24 °C, five independent dialysis experiments were performed, starting from fresh fibrils each time. At 37 °C, two independent dialysis experiments were performed. Absorbance peak volumes at 214 nm were determined using the Beckman-Coulter 32 Karat software package. The corresponding Aβ_{1-40} concentrations were determined from a standard working curve, generated by a series of HPLC measurements on solutions with known concentrations in the 0.5−10 μM range (prepared from DMSO-solubilized Aβ_{1-40}). The smallest Aβ_{1-40} concentration that could be measured reliably was roughly 0.1 μM.

TEM Measurements. TEM images were recorded with an FEI Morgagni microscope operating at 80 kV. For negatively stained images, a 10 μL drop of fibril solution was absorbed for 2 min on a glow-discharged carbon film, supported by lacey carbon on a 300 mesh copper TEM grid. After blotting, the grid was rinsed twice with deionized water and then stained with 10 μL of 3% uranyl acetate for 30 s. The stained solution was blotted, and the grid was dried in air before imaging.

Solid-State NMR. Solid-state ^{15}N and ^{13}C NMR spectra of isotopically labeled fibrils were acquired at ambient temperature in a 9.39 T field (100.4 MHz ^{13}C NMR frequency), using a Varian InfinityPlus spectrometer, a Varian 3.2 mm magic-angle spinning (MAS) NMR probe, and a 9.0 kHz MAS frequency. Standard ^{1}H−^{15}N and ^{1}H−^{13}C cross-polarization and ^{1}H decoupling conditions were employed, with a 1 s delay between scans.

RESULTS

Fibril Morphologies Are Preserved in Seeded Growth. Figure 1A,B shows TEM images of Aβ_{1-40} fibrils after seeded growth in fibril elongation measurements described below. Fibrils grown from $\mathcal{Q}$ or $\mathcal{A}$ fibril seeds retain the characteristic "twisted" and "striated ribbon" morphologies described previously.[2,4] These images verify that the fibrils grown from seeds in our experiments were morphologically homogeneous. TEM images of fibrils used as seeds (before sonication) are shown in Figure S2. Solid-state NMR measurements described below provide additional evidence for morphological homogeneity in our samples. From TEM images, we estimate that morphological homogeneity exceeds 90%.

dx.doi.org/10.1021/ja311963f | J. Am. Chem. Soc. 2013, 135, 6860−6871

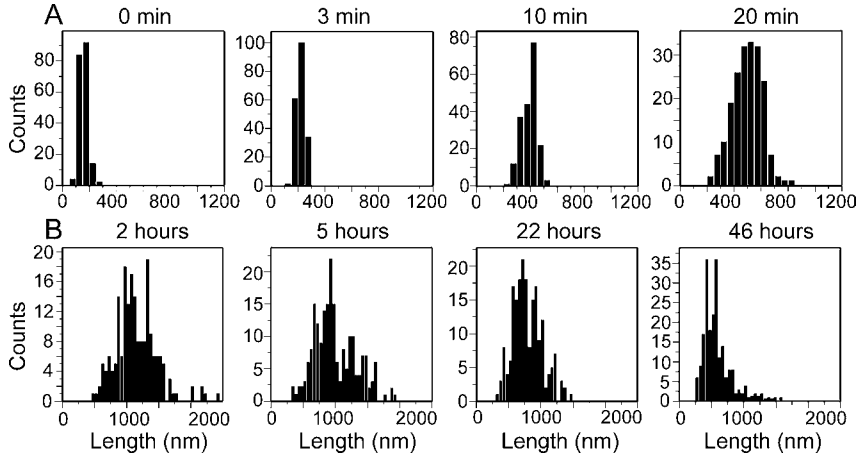

Figure 2. Experimental histograms of $\mathcal{Q}$ fibril lengths from elongation measurements at 24 °C with 50 μM soluble Aβ_{1-40} concentration (A) and from shrinkage measurements (B). Each histogram contains length measurements for 200 individual filaments in the corresponding AFM images.

We emphasize that the terms "$\mathcal{Q}$ fibrils" and "$\mathcal{A}$ fibrils" refer only to the conditions under which seed fibrils were originally prepared. Fibril elongation and shrinkage experiments described below were performed under quiescent conditions for both polymorphs.

Fibril Elongation and Shrinkage at 24 °C Monitored by AFM. AFM has been used extensively by other groups to study the growth and morphology of Aβ fibrils and to identify intermediate species in the assembly process.[6,34−38] Here, we use AFM to measure time-dependent length distributions of Aβ_{1-40} fibrils that grow from seeds with specific structures, after the seeds are added to an Aβ_{1-40} solution with a specific initial concentration. We also use AFM to measure length distributions when fibrils with a specific structure are placed in a monomer-free solution, so that the fibrils dissolve toward the quasi-equilibrium state. Our AFM images were recorded in air, after adsorption of aliquots of fibril-containing Aβ_{1-40} solutions to mica as described above. In principle, time-dependent length distributions could be obtained from images that were recorded in situ (i.e., images of fibrils on the mica surface under the Aβ_{1-40} solution). In our hands, this alternative approach is precluded by instrumental instabilities over long imaging times, fibril fragmentation and desorption induced by the AFM tip, and image degradation due to adherence of Aβ_{1-40} fibrils or other aggregates to the AFM tip. In addition, when fibril elongation and shrinkage are monitored in situ, the possibility exists that interactions with the mica (or other substrate) surface may affect the observations.

Figure 1C,D shows representative AFM images of aliquots of a seeded Aβ_{1-40} solution, taken immediately after seeding (Figure 1C) and 20 min later (Figure 1D). In this case, $\mathcal{Q}$ seeds were used, and the initial soluble Aβ_{1-40} concentration was 50 μM. It is apparent that the seeded solution contained only short fibril fragments initially and that fibrils longer than 1 μm grew from these fragments. In control experiments, no fibrils were observed by TEM or AFM after incubation of an unseeded 50 μM Aβ_{1-40} solution for 30 min. Figure 1E,F shows representative AFM images of a $\mathcal{Q}$ fibril solution after being placed in a monomer-free solution, under dialysis conditions described above. Average fibril lengths after 2 h incubation (Figure 1E) are clearly greater than after 46 h incubation (Figure 1F).

Fibrils in Figure 1D appear to have uniform diameters, with no smaller aggregates associated with them, suggesting an absence of lateral nucleation of Aβ_{1-40} aggregates. In addition, the apparent fibril diameter did not change significantly over 20 min, indicating that linear elongation, rather than self-association or lateral expansion of filaments, was the predominant process.

Figure 2A,B shows histograms of length distributions determined from multiple AFM images under the conditions in Figure 1C−F, for elongation and shrinkage experiments, respectively. Elongation and shrinkage experiments were performed for both $\mathcal{Q}$ and $\mathcal{A}$ fibrils at 24 °C, with initial monomer concentrations of 25, 50, and 75 μM in the elongation experiments. Additional AFM images and length histograms from these experiments are shown in Figures S3 and S4. Interestingly, in all elongation experiments, in addition to the expected monotonic increase in the average fibril length, we observed that the width of the length distribution increased with increasing incubation time. This observation is discussed further below.

Kinetics and Thermodynamics from AFM and UV. Figure 3A,B shows plots of average fibril lengths as a function of incubation time in elongation experiments. For each value of the initial Aβ_{1-40} monomer concentration, fibril lengths increase linearly with time. As shown in Figure 3C, the slope increases linearly with monomer concentration. (Linear fits in Figure 3C were constrained to pass through the origin, an approximation that is justified by the small experimental values of k_s.) Figure 3D shows that the average fibril length decreases linearly with incubation time in shrinkage experiments. Slopes from Figure 3C,D represent values of k_e and k_s in eq 1. These values are given in Table 1, along with values of $M_{QE,AFM} = k_s/k_e$. Interestingly, elongation and shrinkage rates for $\mathcal{A}$ fibrils are both significantly larger than the corresponding rates for $\mathcal{Q}$ fibrils, but the values of $M_{QE,AFM}$ are nearly the same. Error limits on k_s and k_e represent standard errors reported by the Origin 6.0 software (OriginLab Corp.) used to fit the data. Given these error limits, the resulting values of $M_{QE,AFM}$ are not significantly different.

Linear dependence of the average fibril length on time is predicted by eq 1, provided that M does not change appreciably over the measurement time, which is the case in our experiments. Linear dependence of the elongation rate on soluble peptide concentration is expected under conditions that are explained in the Discussion section.

dx.doi.org/10.1021/ja311963f | J. Am. Chem. Soc. 2013, 135, 6860−6871

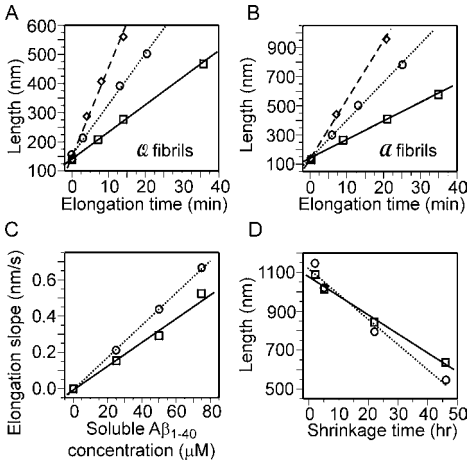

Figure 3. (A,B) Plots of experimental average fibril lengths and best-fit lines as a function of elongation time for $\mathcal{Q}$ and $\mathcal{A}$ Aβ_{1-40} fibrils. Experiments were done with 25 μM (squares and solid lines), 50 μM (circles and dotted lines), and 75 μM (diamonds and dashed lines) soluble Aβ_{1-40} concentrations. (C) Experimental elongation slopes as a function of soluble Aβ_{1-40} concentration and best-fit lines for $\mathcal{Q}$ (squares and solid lines) and $\mathcal{A}$ (circles and dotted lines) fibrils. (D) Plots of experimental average fibril lengths and best-fit lines as a function of shrinkage time for $\mathcal{Q}$ (squares and solid lines) and $\mathcal{A}$ (circles and dotted lines) fibrils. Experiments were done at 24 °C. Experimental errors are approximately equal to the symbol sizes.

Quasi-equilibrium solubilities were also determined from dialysis experiments under conditions similar to the fibril shrinkage experiments, but with a larger initial quantity of fibrils in the dialysis tube, so that quasi-equilibrium between fibrillar and soluble Aβ_{1-40} was established over the entire dialysis system within 72 h. Values of $M_{QE,UV}$ in Table 1 were then determined from UV absorbance of the solution outside the dialysis tube, using analytical HPLC. HPLC traces are shown in Figure S5. Values of $M_{QE,AFM}$ and $M_{QE,UV}$ agree to within the errors in each measurement. The combined results from AFM and UV suggest that $\mathcal{A}$ fibrils may be more stable than $\mathcal{Q}$ fibrils. This suggestion is supported by solid-state NMR data described below.

In elongation experiments, the average fibril lengths increased by 400−800 nm during the measurement time. Given an initial 20-fold excess of soluble Aβ_{1-40} over fibrillar Aβ_{1-40} and an initial average fibril length of 150 nm, this implies that 20% or less of the soluble Aβ_{1-40} was consumed during the measurement time. In principle, consumption of soluble Aβ_{1-40} would cause the data in Figure 3A,B to depart from linearity. Under our conditions, consumption of soluble Aβ_{1-40} affects slopes determined by linear fits to the data by 5% or less. (In preliminary experiments, departure from linearity was observed at longer times, particularly at the higher soluble Aβ_{1-40} concentrations.)

In shrinkage experiments, the volume of the buffer reservoir and the initial quantity of fibrils were chosen so that the Aβ_{1-40} monomer concentration would be ∼0.15 μM if all fibrils dissolved completely. Based on the measured length distributions, less than half of the total fibril mass dissolved during shrinkage measurements. Control experiments shown in Figure S5 confirmed that monomeric Aβ_{1-40} diffused out of the dialysis tube on the time scale of 2 h, much less than the time scale for fibril shrinkage. Thus, the shrinkage kinetics were not affected by the presence of the dialysis membrane between the fibrils and the buffer reservoir.

Temperature Dependence of Kinetics and Thermodynamics. Fibril elongation and shrinkage experiments were also performed at 37 °C. Fibril length distributions from elongation experiments are shown in Figure S6. Plots of the dependences of average fibril lengths on incubation time and the dependence of the elongation slope on initial monomer concentration are shown in Figure 4. As shown in Table 1, values of k_s decrease by factors of roughly 1.5, and values of k_e increase by factors of 4−6 as temperature increases from 24 to 37 °C. As a result, values of $M_{QE,AFM}$ decrease by factors of 6−9 and become less

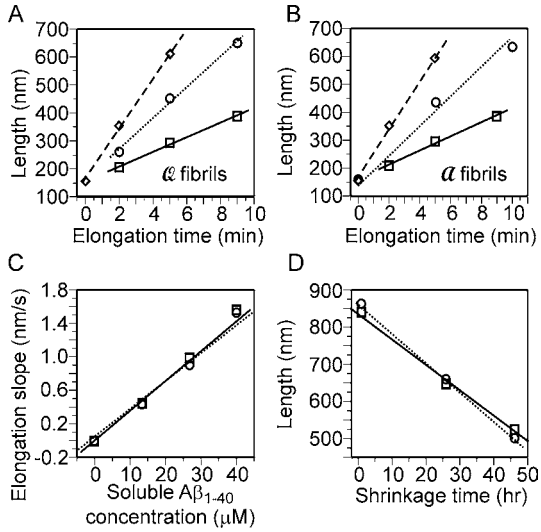

Figure 4. Similar plots as in Figure 3, but for experiments done at 37 °C. Soluble Aβ_{1-40} concentrations in panels A and B are 13.3 μM (squares and solid lines), 26.7 μM (circles and dotted lines), and 40.0 μM (diamonds and dashed lines).

Table 1. Kinetic Parameters and Quasi-Equilibrium Aβ_{1-40} Monomer Concentrations for $\mathcal{Q}$ and $\mathcal{A}$ Fibrils Determined by AFM and UV Absorbance

temperature	fibril type	k_e (nm/s·μM)	k_s (nm/s)	$M_{QE,AFM}$ (μM)	$M_{QE,UV}$ (μM)[a,b]
24 °C	$\mathcal{Q}$	$(6.07 \pm 0.23) \times 10^{-3}$	$(2.71 \pm 0.19) \times 10^{-3}$	0.45 ± 0.04	0.50 ± 0.08
	$\mathcal{A}$	$(8.68 \pm 0.11) \times 10^{-3}$	$(3.44 \pm 0.36) \times 10^{-3}$	0.40 ± 0.04	0.34 ± 0.06
37 °C	$\mathcal{Q}$	$(35.5 \pm 1.8) \times 10^{-3}$	$(1.89 \pm 0.13) \times 10^{-3}$	0.053 ± 0.005	–
	$\mathcal{A}$	$(35.0 \pm 2.0) \times 10^{-3}$	$(2.21 \pm 0.02) \times 10^{-3}$	0.063 ± 0.004	–

[a]Uncertainties in $M_{QE,UV}$ represent the standard deviation from five independent measurements. [b]$M_{QE,UV}$ at 37 °C was below our detection limit.

dx.doi.org/10.1021/ja311963f | J. Am. Chem. Soc. 2013, 135, 6860−6871

than the 0.1 μM detection limit of our UV/HPLC measurements. Indeed, attempts to measure $M_{QE,UV}$ were unsuccessful (see Figure S5). At 37 °C, the difference between $M_{QE,AFM}$ values for $\mathcal{Q}$ and $\mathcal{A}$ fibrils is not larger than experimental uncertainties.

Simulations of Intermittent Fibril Elongation. As shown in Figures 2, S3, and S5, the widths of fibril length distributions in elongation experiments clearly increase with increasing incubation time. If elongation and shrinkage rates of individual fibrils are constant (with these rates defined as the probabilities of adding or subtracting a monomer in a very small time interval, divided by the time interval, and multiplied by the length change λ per monomer), then one expects the average fibril length to increase as $(k_eM - k_s)t$, where t is the incubation time, M is the monomer concentration, and the width of the length distribution to increase is $[\lambda(k_eM + k_s)t]^{1/2}$. Thus, the ratio of the width of the distribution to the average fibril length should decrease with increasing incubation time in elongation experiments, contrary to our experimental results. This observation suggests that elongation rates of individual fibrils are not constant.

To explain the observed length distributions, we invoke a model in which individual filaments switch between "on" and "off" states, with correlation time τ_c and fractional occupancies f_{on} and $f_{off} = 1 - f_{on}$. In the "on" state, fibrils elongate at the rate $k_{on} = k_eM/f_{on}$, where k_e is the experimentally determined value; in the "off" state, fibrils do not elongate. This model is supported by previous studies of Aβ and glucagon fibrils, which provided direct evidence for intermittent fibril growth from in situ fluorescence microscopy[31,32] and AFM[30] imaging. To estimate the values of f_{on} and τ_c for Aβ_{1-40} fibril growth under our experimental conditions, we simulated fibril length distributions as follows: (i) In each elongation simulation, we calculated the growth of 200 independent fibrils, with an initial length distribution equal to the experimental length distribution at $t = 0$. (ii) The initial state of each fibril was randomly chosen to be "on" or "off", with probabilities f_{on} and f_{off}. (iii) The incubation period was divided into time steps $\delta t = 1$ s. At each time step, the state of the fibril was allowed to change, based on random numbers, with probabilities equal to $[1 - \exp(-t'/\tau_c)]$ f_{off} for changing from "on" to "off" and $[1 - \exp(-t'/\tau_c)]f_{on}$ for changing from "off" to "on", where t' is the time since the previous change in state. (iv) The fibril length at time t was then equal to its initial length plus $n_{on}(t)k_{on}\delta t$, where $n_{on}(t)$ is the number of time steps in which the fibril was in the "on" state up to time t. (v) For each experimental condition and each choice of f_{on} and τ_c, the results of 50 independent simulations, with different random number choices, were averaged. The shrinkage rate k_s was not included in these simulations, because shrinkage is negligible on the time scale of our elongation experiments. Simulated length distributions were then compared with experimental distributions by calculating the total squared deviation Δ^2 between simulated and experimental length histograms at all incubation times for a given experimental condition.

Figure 5 compares experimental and best-fit simulated length distributions at 9, 21, and 35 min incubation times for $\mathcal{A}$ fibrils with 25 μM initial soluble Aβ_{1-40} concentration at 24 °C. Figures S4 and S6 show the full set of experimental and simulated distributions. Agreement between experiments and simulations is good, indicating that the intermittent elongation model can explain the observed broadening of fibril length distributions. Figures 6 and S7 show contour plots of Δ as a function of τ_c and f_{on}, from which the best-fit parameters and their uncertainties given in Table 2 were determined. Best-fit values of f_{on} are in the 0.3−0.7 range. Values of τ_c are in the 10−70 s range, with the smaller values occurring at 37 °C.

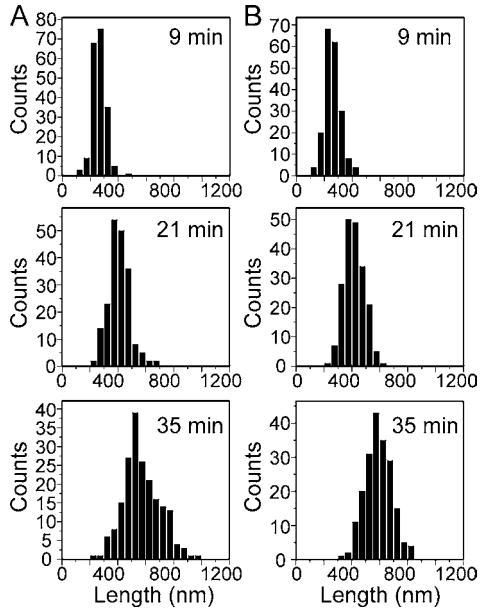

Figure 5. Experimental (A) and best-fit simulated (B) histograms of $\mathcal{A}$ fibril lengths in elongation measurements with 25 μM soluble Aβ_{1-40} concentration (τ_c = 41 s and f_{on} = 0.36 in simulations).

Structural Interconversion Monitored by Solid-State NMR. At 24 °C, values of M_{QE} derived from both AFM and UV measurements are smaller for $\mathcal{A}$ fibrils than for $\mathcal{Q}$ fibrils, although the uncertainties in these measurements preclude a definite conclusion regarding the relative thermodynamic stabilities of the two polymorphs. Based on results in Table 1, the ratio of the M_{QE} value for $\mathcal{Q}$ fibrils to the M_{QE} value for $\mathcal{A}$ fibrils may be as large as 2.0 at 24 °C. Assuming that the chemical potential for soluble Aβ_{1-40} is given by the expression $\mu_S = \mu_S^* + RT\ \ln(M/M^*)$, where M is the concentration in solution and μ_S^* is the chemical potential at a reference concentration M^*, and assuming that the chemical potential of Aβ_{1-40} in a specific fibril polymorph at quasi-equilibrium equals the chemical potential in solution at concentration M_{QE}, the difference in chemical potentials in $\mathcal{Q}$ and $\mathcal{A}$ fibrils is $\Delta\mu_F = RT\ \ln[M_{QE}(\mathcal{Q})/M_{QE}(\mathcal{A})]$. Using values in Table 1, $\Delta\mu_F$ may be as large as 0.8 kcal/mol or as small as −0.08 kcal/mol at 24 °C.

Provided that $\Delta\mu_F \neq 0$, a 1:1 mixture of $\mathcal{Q}$ and $\mathcal{A}$ fibrils should evolve toward the more stable structure by gradual net shrinkage of the less stable fibrils and net elongation of the more stable fibrils. Eventually, the less stable fibrils should disappear (even if $\Delta\mu_F$ is very small, because it is always thermodynamically favorable to transfer Aβ_{1-40} molecules from a less stable to a more stable polymorph, assuming that the chemical potentials are independent of fibril length). The time scale for this process can be estimated as follows: Assuming that the 1:1 mixture contains equal numbers of $\mathcal{Q}$ and $\mathcal{A}$ fibrils, a steady-state monomer concentration will be established in which the average number of monomers in the more stable fibrils increases at the same rate at which the average number of monomers in the less stable fibrils decreases. One can show that this rate (in monomers per second) equals $\eta_A\eta_Q(k_{eQ}k_{sA} - k_{eA}k_{sQ})/(\eta_Qk_{eQ} + \eta_Ak_{eA}) \equiv k_{mix}$, where subscripts A and Q refer

dx.doi.org/10.1021/ja311963f | J. Am. Chem. Soc. 2013, 135, 6860−6871

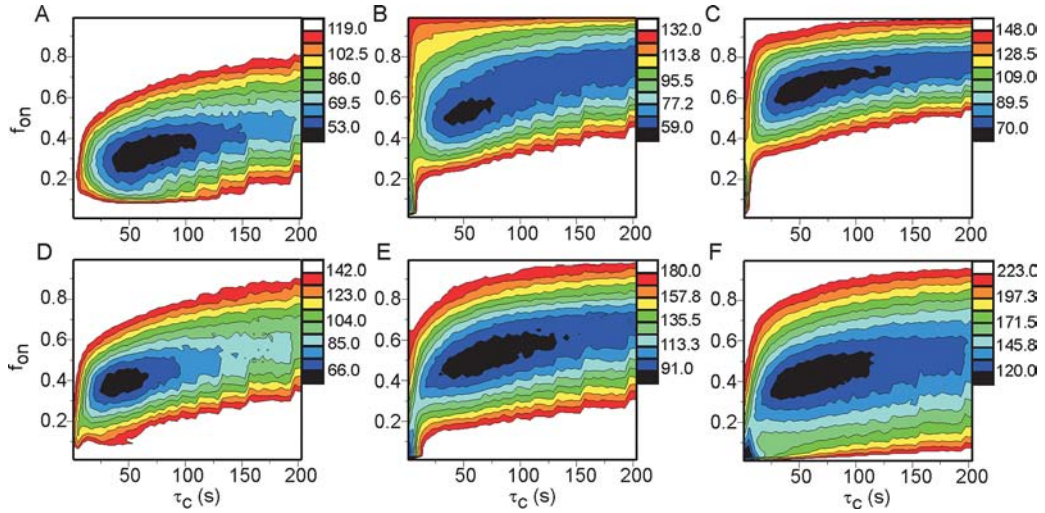

Figure 6. Contour plots of the deviation between experimental and simulated histograms of Aβ_{1-40} fibril length distributions in fibril elongation measurements at 24 °C, as a function of the correlation time (τ_c) and elongation fraction (f_{on}) assumed in the simulations. (A,B,C) $\mathcal{Q}$ fibrils with 25, 50, and 75 μM soluble Aβ_{1-40} concentrations, respectively. (D,E,F) $\mathcal{A}$ fibrils with 25, 50, and 75 μM soluble Aβ_{1-40} concentrations, respectively. Each contour plot represents the average of 50 independent simulations with different random numbers to determine switching of fibrils between "on" and "off" elongation states. In each plot, the contour level increment was set to $(2\Delta^2_{min})^{1/2}$, where Δ^2_{min} was the minimum total squared deviation between simulated and experimental histograms.

Table 2. Best-Fit Elongation Fraction (f_{on}) and Correlation Time (τ_c) Values in Simulations of Aβ_{1-40} Fibril Elongation Measurements

temperature	fibril type	initial monomer concentration (μM)	f_{on}[a]	τ_c (s)[a]
24 °C	$\mathcal{Q}$	25	0.35 ± 0.09	77 ± 35
		50	0.57 ± 0.07	61 ± 21
		75	0.69 ± 0.07	65 ± 40
	$\mathcal{A}$	25	0.39 ± 0.05	37 ± 18
		50	0.49 ± 0.09	57 ± 42
		75	0.41 ± 0.08	57 ± 40
37 °C	$\mathcal{Q}$	13	0.40 ± 0.10	19 ± 9
		27	0.42 ± 0.17	12 ± 8
		40	0.61 ± 0.11	47 ± 32
	$\mathcal{A}$	13	0.45 ± 0.13	23 ± 12
		27	0.39 ± 0.19	15 ± 7
		40	0.63 ± 0.18	50 ± 40

[a]Uncertainties represent ranges of variation for individual parameters within which the total squared deviation between experimental and simulated length histograms does not exceed $\Delta^2_{min} + (2\Delta^2_{min})^{1/2}$.

to the two polymorphs and η is the number of monomers per nm. From Table 1, with η_A = 4.2/nm and η_Q = 6.3/nm (corresponding to 2- and 3-fold symmetric structures with a 0.48 nm repeat distance), the value of k_{mix} may be roughly 5×10^{-4} s^{-1}, corresponding to a time of roughly 2×10^6 s, or 22 days, for $\mathcal{Q}$ fibrils to shrink by 150 nm. The actual time scale is sensitive to the precise values of k_e and k_s.

To test for interconversion between $\mathcal{Q}$ and $\mathcal{A}$ fibril structures experimentally, we recorded solid-state ^{13}C and ^{15}N NMR spectra of $\mathcal{Q}$ and $\mathcal{A}$ fibrils and a mixture of the two polymorphs. For these measurements, Aβ_{1-40} was synthesized with uniform ^{15}N and ^{13}C labeling of a single residue, namely I32. Labeled $\mathcal{Q}$ fibrils were grown from seeds. Labeled $\mathcal{A}$ fibrils were grown de novo, with agitation as described above. Fibrils (3 mg of each polymorph) were pelleted by ultracentrifugation (435 000 × g, 3 h) and loaded into separate MAS rotors by centrifugation (14 000 × g). After recording NMR spectra of each polymorph separately, the fibrils were removed from the rotors, resuspended together in 200 μL of incubation buffer, pelleted again, and reloaded into a single MAS rotor. NMR spectra of the mixture were recorded immediately. Fibrils were then removed from the rotor, resuspended in 500 μL of incubation buffer, sonicated to produce fragments with lengths of ∼50 nm (Branson model S-250A sonifier with tapered 1/8″ microtip horn, lowest power, 10% duty cycle, 10 min), and incubated at 24 °C for 35 days. During the incubation period, the fibrils were sonicated again for 2 min on days 3, 6, 9, and 12. Sonication was performed to ensure that all fibrils remained short, thereby accelerating the interconversion process. After 35 days, fibrils were pelleted again and reloaded into a single MAS rotor. Due to sample losses during unpacking and repacking of the MAS rotor, the final set of spectra required a total of 5.5 days of signal averaging. Earlier spectra were recorded in <1 day.

^{15}N NMR spectra are shown in Figure 7A. The backbone amide ^{15}N chemical shifts for I32 in $\mathcal{Q}$ and $\mathcal{A}$ fibrils differ by 2.65 ppm, allowing signal contributions from the two polymorphs to be resolved in spectra of the mixture. Deconvolution of the ^{15}N NMR spectra shows that the ratio $\mathcal{A}$ fibril mass to $\mathcal{Q}$ fibril mass in the mixture was initially 1.3:1.0. After 35 days of incubation at 24 °C, this ratio changed to 2.6:1.0. Thus, $\mathcal{A}$ fibrils have greater thermodynamic stability than $\mathcal{Q}$ fibrils under our experimental conditions, as suggested by the values of M_{QE} in Table 1. The long time scale required for interconversion (>35 days for completion) is consistent with the estimate derived above.

^{13}C NMR spectra are shown in Figure 7A–C. Most ^{13}C sites in I32 have nearly identical chemical shifts in the two polymorphs. The largest difference occurs at the backbone carbonyl site. Although carbonyl ^{13}C NMR lines of $\mathcal{Q}$ and $\mathcal{A}$ fibrils overlap in spectra of the mixture, changes in the carbonyl line shape shown in Figure 7C indicate a greater ratio of $\mathcal{A}$ fibril mass to $\mathcal{Q}$ fibril mass after 35 days, consistent with conclusions from the ^{15}N NMR spectra. In the aliphatic region of the ^{13}C NMR spectra (Figure 7D), α-carbon signals of I32

dx.doi.org/10.1021/ja311963f | J. Am. Chem. Soc. 2013, 135, 6860–6871

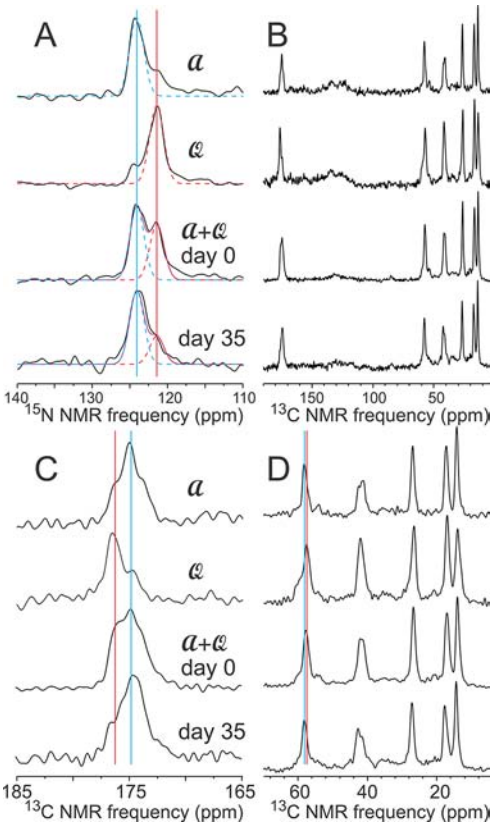

Figure 7. (A) Solid-state ^{15}N NMR spectra of Aβ_{1-40} fibrils, with uniform ^{15}N and ^{13}C labeling of I32. Spectra of $\mathcal{A}$ and $\mathcal{Q}$ fibrils and a mixture of $\mathcal{A}$ and $\mathcal{Q}$ fibrils after 0 and 35 days of incubation at 24 °C are shown. Dashed blue and red lines are Gaussian lineshapes with full-width-at-half-maximum equal to 2.22 ppm, fitted to ^{15}N signals of $\mathcal{A}$ and $\mathcal{Q}$ fibrils, respectively. Blue and red vertical lines indicate peak positions for signals from $\mathcal{A}$ and $\mathcal{Q}$ fibrils. Spectra of the mixture indicate gradual transfer of Aβ_{1-40} from $\mathcal{Q}$ fibrils to $\mathcal{A}$ fibrils, confirming the greater thermodynamic stability of $\mathcal{A}$ fibrils under these experimental conditions. (B) Solid state ^{13}C NMR spectra of the same samples. (C) Expansions of carbonyl regions of the ^{13}C NMR spectra. (D) Expansions of aliphatic regions of the ^{13}C NMR spectra. (Note that up to 5% of the ^{15}N NMR signal amplitude and up to 33% of the carbonyl ^{13}C NMR signal amplitude arises from natural abundance ^{15}N and ^{13}C at residues other than I32.).

appear near 58 ppm, with a 0.7 ppm difference between chemical shifts of $\mathcal{Q}$ and $\mathcal{A}$ fibrils. After 35 days, the peak position of the α-carbon line in the spectrum of the mixture agrees well with the peak position in the spectrum of $\mathcal{A}$ fibrils, again consistent with conclusions from the ^{15}N NMR spectra.

Polymorphic-Specific Susceptibility of Aβ_{1-40} Fibrils to Fragmentation. As discussed by others, fibril growth can be influenced by mechanical properties, especially susceptibility to fragmentation, since fragmentation creates new fibril ends and therefore accelerates the net growth of fibril mass.[39,40] To test for differences in susceptibility to fragmentation, we exposed $\mathcal{Q}$ and $\mathcal{A}$ fibrils to shear forces, by placing fibril solutions in vials that contained rapidly rotating stir bars. As shown in Figure S8, $\mathcal{A}$ fibrils were found to be significantly more susceptible to fragmentation by shear forces than were $\mathcal{Q}$ fibrils, breaking into <1 μm segments within 15 min (compared with several hours for $\mathcal{Q}$ fibrils). This result may arise from the fact that fragmentation of $\mathcal{A}$ fibrils requires disruption of approximately two-thirds as many intermolecular interactions, including backbone hydrogen bonds and side chain−side chain interactions, as does fragmentation of $\mathcal{Q}$ fibrils.

DISCUSSION

Summary of Results. Our results show that AFM images can be used to quantify time-dependent Aβ_{1-40} fibril length distributions, allowing the determination of rates of fibril extension and shrinkage in the presence and absence of excess soluble Aβ_{1-40}. Growth rates are proportional to the concentration of excess soluble Aβ_{1-40}. The soluble Aβ_{1-40} concentration at quasi-equilibrium, M_{QE}, is then given by the ratio of rate constants for shrinkage and extension, k_s/k_e. Values of M_{QE} determined in this way are in good agreement with direct measurements by UV absorbance, providing validation for both approaches. In principle, the AFM approach has several advantages: (i) it is not necessary for a quasi-equilibrium state to be reached, as long as k_s and k_e are measurable; (ii) it is not necessary for fibrils to be separated from soluble species; (iii) both kinetic information and thermodynamic information are obtained; (iv) small values of M_{QE}, below the detectable limit of our UV measurements, can be determined; (v) impurities that do not interact with Aβ_{1-40} fibrils but may interfere with UV measurements, such as low levels of oxidized or racemized Aβ_{1-40}, do not affect the AFM measurements. For UV absorbance measurements, we have developed a simple dialysis approach that obviates the need to separate soluble from fibrillar peptide (by ultracentrifugation, filtration, or some other method) and allows periodic monitoring of the fibril dissolution process.

Results in Table 1 show that two Aβ_{1-40} fibril polymorphs with distinct molecular structures have very similar values of M_{QE} and hence similar thermodynamic stabilities. However, at 24 °C, values of k_e and (possibly) k_s are significantly greater for $\mathcal{A}$ fibrils than for $\mathcal{Q}$ fibrils. This difference in kinetics may be related to structural differences. In particular, $\mathcal{Q}$ and $\mathcal{A}$ fibrils have mass-per-length values of ∼27 and ∼18 kDa/nm, respectively, corresponding to molecular structures with 3- or 2-fold symmetry about the fibril growth axis.[2−4,20] If the rates of addition of Aβ_{1-40} monomers to the ends of the two polymorphs were the same, values of k_e (in length units, rather than monomer units) would be in a 3:2 ratio, close to experimental observations. At 37 °C, values of k_e and k_s are very similar, indicating that this simple structural argument has limited validity.

Both AFM and UV measurements suggest that $\mathcal{A}$ fibrils may be more stable than $\mathcal{Q}$ fibrils at 24 °C, by up to 0.8 kcal/mol. Direct measurements of interconversion between the two polymorphs, monitored by solid-state NMR spectroscopy over a period of 35 days as shown in Figure 7, confirm that $\mathcal{A}$ fibrils are more stable.

Values of M_{QE} are roughly 8 times smaller at 37 °C than at 24 °C, an observation that is consistent with stabilization of Aβ_{1-40} fibril structures by hydrophobic interactions, as indicated by early biochemical studies[41−43] and later structural studies.[3,4,8,44] The lower values at the more physiologically relevant temperature may have implications for fibril formation in AD. Soluble Aβ_{1-40} and Aβ_{1-42} concentrations in brain tissue of AD patients have been reported to be roughly 5−10 nM.[45] Of course, we expect quasi-equilibrium solubilities to be affected also by ionic strength, association with membrane surfaces, macromolecular crowding, and other physiological factors.

dx.doi.org/10.1021/ja311963f | J. Am. Chem. Soc. 2013, 135, 6860−6871

Kinetic Model. Fibril growth rates are much less than diffusion-limited rates. With a translational diffusion constant for Aβ_{1-40} of 1.5×10^{-6} cm^2/s,[46] the diffusion-limited rate of attachment of new monomers to the ends of a fibril can be estimated to be roughly 1×10^3/s·μM.[47] With a repeat distance of 0.48 nm in a cross-β amyloid structure and with either two or three monomers per repeat unit, the diffusion-limited value of k_e is roughly 200 nm/s·μM, much greater than experimentally observed values in Table 1. Therefore, only a small fraction ($\sim 10^{-4}$) of collisions between monomers and fibril ends lead to fibril growth. Given that Aβ_{1-40} is conformationally disordered in its soluble state and becomes conformationally ordered in its fibrillar state, it seems likely that monomers bind initially to fibril ends in a somewhat disordered state and in a transient manner, before adopting the fibrillar conformation. Such behavior is observed in simulations of monomer/fibril interactions,[48−50] and may be related to the "dock-lock" mechanism of fibril growth proposed by Esler et al.[29] (see below).

A simple kinetic scheme (eq 2) that corresponds to transient binding of disordered monomers before their incorporation into the fibril structure is the following:

$$\mathrm{M} + \mathrm{F}_n \underset{k_{-1}}{\overset{k_1}{\rightleftarrows}} \mathrm{M^*F}_n \underset{k_{-2}}{\overset{k_2}{\rightleftarrows}} \mathrm{F}_{n+1} \tag{2}$$

where M represents a free monomer, F_n represents a fibril containing n structured monomers, and M^*F_n represents a fibril containing n structured monomers with an additional unstructured monomer bound to its end. Equation 2 implies

$$\frac{\mathrm{d}[M^*F_n]}{\mathrm{d}t} = k_1[M][F_n] - k_{-1}[M^*F_n] - k_2[M^*F_n] + k_{-2}[F_{n+1}] \tag{3}$$

Under conditions of steady-state growth, $\sum_{n=1}^{\infty}(\mathrm{d}[M^*F_n]/\mathrm{d}t) = 0$. Defining the total fibril concentration to be $[F_T] \equiv \sum_{n=1}^{\infty}\{[F_n] + [M^*F_n]\}$ and the total concentration of fibril-bound unstructured monomers to be $[M^*F] \equiv \sum_{n=1}^{\infty}[M^*F_n]$, and assuming $[F_1]$ to be negligible, eq 3 then implies

$$[M^*F] = \frac{\{k_1[M] + k_{-2}\}[F_T]}{k_1[M] + (k_{-1} + k_2 + k_{-2})} \tag{4}$$

The net fibril growth rate k_{growth} (in monomers per unit time) is the difference between the total rate of conversion from M^*F_n to F_{n+1} and the total rate of conversion from F_{n+1} to M^*F_n, summed over n:

$$k_{growth} = k_2[M^*F] - k_{-2}\{\sum_{n=1}^{\infty} F_{n+1}\} \tag{5a}$$

$$= \left\{\frac{(k_2 + k_{-2})(k_1[M] + k_{-2})}{k_1[M] + (k_{-1} + k_2 + k_{-2})} - k_{-2}\right\}[F_T] \tag{5b}$$

The expression for k_{growth} in eq 5b is analogous to standard expressions for rates of enzymatic catalysis, with $[M]$ taking the place of the substrate concentration and $[F_T]$ taking the place of the total enzyme concentration.[51] In the limit that $[M]$ is sufficiently small that fibril ends are not saturated with unstructured monomers (i.e., $k_1[M] \ll k_{-1}$), yet sufficiently large that fibril elongation dominates over fibril shrinkage, eq 5b predicts that the fibril growth rate is proportional to the monomer concentration, in agreement with our experiments (see Figures 3C and 4C). In the context of this kinetic model, and assuming $k_2 \gg k_{-2}$, our measured values of k_e and k_s correspond to $\eta k_e \approx k_2k_1/k_{-1}$ and $\eta k_s \approx k_{-2}$, where η is the number of monomers per nm. The fraction of fibrils with a bound, unstructured monomer is $[M^*F]/[F_T] \approx k_1[M]k_{-1}$, which can not be determined from k_e and k_s.

We note that the foregoing analysis assumes that fibrils have only one actively growing end, an assumption that can be easily removed. For simplicity, we assume that fibril ends accommodate only one unstructured monomer, although the experimentally based structural models for $\mathcal{Q}$ and $\mathcal{A}$ fibrils and experimental mass-per-length data indicate multiple monomers per repeat unit. More complicated kinetic models can treat a situation in which two or more unstructured monomers must bind before the structurally ordered fibril length can increase. In the absence of information about the molecular structure at fibril ends, which is likely to differ from the bulk structure, we have not pursued such models.

Intermittent Fibril Elongation. Fibril length distributions increase in width with increasing time in elongation experiments, more rapidly than expected if elongation were proceeding at a constant rate. As shown in Figures 5, S4, and S6, the length distributions can be explained by assuming that fibrils grow intermittently, as observed for Aβ_{1-40} and other fibrils in earlier studies.[30−32] A likely physical mechanism for intermittent elongation is that molecules at the fibril ends occasionally adopt a stable structure that differs from the bulk structure and can not propagate, effectively capping the fibril ends. Fits to the length distributions in Figures 6 and S7 and Table 2 indicate that fibrils may be capped in this way 20−80% of the time, with no clear correlation between f_{on} and monomer concentration, temperature, or fibril structure. The correlation time for switching between elongating and capped states is 10−70 s, apparently somewhat smaller at 37 °C than at 24 °C, suggesting that switching between states is a thermally activated process. Values of k_s in Table 1 indicate that structured Aβ_{1-40} monomers dissociate from fibrils at $(1-2) \times 10^{-2}$ s^{-1} rates in the absence of soluble Aβ_{1-40}, corresponding to lifetimes that are comparable to the values of τ_c in Table 2.

Intermittent elongation could be included in the kinetic scheme discussed above by adding a capped state M^*F_n that exchanges with M^*F_n at forward and reverse rates on the order of $1/\tau_c$ but does not convert to F_{n+1}. It is worth emphasizing that the existence of capped states and intermittent elongation does not invalidate the equality of k_s/k_e and M_{QE}, because the quasi-equilibrium solubility is determined by time-averaged elongation and shrinkage rates that already include intermittency.

Factors Influencing Fibril Polymorphism. One motivation for investigating polymorph-specific thermodynamics and kinetics of Aβ_{1-40} fibril formation is to improve our understanding of how certain growth conditions favor certain polymorphs in de novo (i.e., unseeded) fibril preparations. In particular, the predominant fibril structure in de novo preparations has two-fold symmetry when the Aβ_{1-40} solution is agitated during fibril growth and three-fold symmetry when the solution is quiescent, all other conditions being the same (pH 7.4, 24 °C, 10 mM phosphate buffer).[2] In principle, the predominant structure under a given set of experimental conditions could be determined by kinetic factors (i.e., rates of nucleation and elongation) or by thermodynamic stability. Experiments described above show that the thermodynamic

dx.doi.org/10.1021/ja311963f | J. Am. Chem. Soc. 2013, 135, 6860−6871

stabilities and elongation rates of $\mathcal{Q}$ and $\mathcal{A}$ fibrils are rather similar, indicating that these factors do not explain why $\mathcal{Q}$ or $\mathcal{A}$ fibrils predominate under specific conditions. On the other hand, $\mathcal{Q}$ and $\mathcal{A}$ fibrils have significantly different susceptibilities to fragmentation under shear forces. In agitated solutions, where shear forces are similar in magnitude to those in experiments shown in Figure S8, preferential fragmentation of $\mathcal{A}$ fibrils is expected to accelerate the net growth of these fibrils relative to the net growth of $\mathcal{Q}$ fibrils, leading to the predominance of $\mathcal{A}$ fibrils. The predominance of $\mathcal{Q}$ fibrils in quiescent solutions, where shear forces are negligible, is explicable if the intrinsic nucleation rate of $\mathcal{Q}$ fibrils exceeds that of $\mathcal{A}$ fibrils.

It is additionally possible that nucleation of $\mathcal{A}$ fibrils occurs at interfaces, either between the Aβ_{1-40} solution and air or between the peptide solution and the walls of the tube. Under agitated growth conditions (see Materials and Methods), the surface-to-volume ratio of the solution is increased, potentially accelerating interface-dependent nucleation.

The similarity of thermodynamic stabilities of $\mathcal{Q}$ and $\mathcal{A}$ fibrils helps explain why polymorphism is a prevalent phenomenon in studies of amyloid fibrils. Similar M_{QE} values (i.e., similar values of k_e/k_s, which in turn leads to small values of k_{mix}) for structurally distinct fibrils imply that interconversion among polymorphs is a slow process, especially after fibrils grow to micrometer-scale lengths. Thus, a mixture of polymorphs will not evolve to a structurally homogeneous state on the time scale of typical in vitro experiments. The low M_{QE} values of various polymorphs also imply that, once a quasi-equilibrium state is reached, nucleation of a new polymorph (even a more thermodynamically stable one) will occur at a very low rate. It is therefore essentially impossible for a sample of amyloid fibrils to evolve to its true equilibrium state on a realistic time scale, unless the most thermodynamically stable fibril structures are already present in the sample.

Comparisons with Previous Kinetic and Thermodynamic Studies. Values of M_{QE} for Aβ_{1-40} fibrils, also called "critical concentrations", have been determined previously by several groups, either from direct measurements of soluble Aβ_{1-40} concentrations at quasi-equilibrium[7,23−25,52,53] or from kinetic measurements based on surface plasmon resonance[26,27] (SPR) or quartz crystal microbalance[28] (QCM) data. Reported values cover a wide range, from below 0.1 μM[24,26] to above 10 μM.[25,53] Some of this variation may be due to incomplete establishment of quasi-equilibrium, incomplete separation of aggregated Aβ_{1-40} from soluble Aβ_{1-40}, or other experimental uncertainties. In addition, it is likely that different studies involved different polymorphs and that fibrils were structurally heterogeneous in some of these studies. Although we find that $\mathcal{Q}$ and $\mathcal{A}$ fibrils have similar M_{QE} values, other polymorphs may have significantly different values. Kodali et al. have observed values ranging from 0.23 μM to 16 μM for distinct Aβ_{1-40} fibril polymorphs in phosphate buffer at 37 °C.[7]

Previous kinetic studies of seeded Aβ_{1-40} fibril growth have also yielded variable results. The linear dependence of elongation rate on soluble Aβ_{1-40} concentration in our experiments has been seen in most previous studies,[26−28,46] but not all.[31] From quasi-elastic light scattering data, Lomakin et al. inferred an elongation rate (ηk_e) equal to 6.5×10^{-5} μM^{-1} s^{-1} in 0.1 M HCl,[54] significantly smaller than the values in our experiments near neutral pH. Kinetic data from SPR[26,27] and QCM[28] studies do not provide estimates of absolute k_e and k_s values, due to the unknown coverages and lengths of fibrils in those studies. Using fluorescence microscopy, Ban et al. observed intermittent Aβ_{1-40} fibril growth, with an average elongation rate of ∼5 nm/s at pH 7.5, 37 °C, and 50 μM soluble Aβ_{1-40} concentration,[31] which corresponds to a k_e value roughly three times larger than values in Table 1. By analyzing hydrogen/deuterium exchange data attributed to continual dissociation and reassociation of monomers at fibril ends under quasi-equilibrium conditions, Sanchez et al. derived a dissociation/reassociation rate of 0.6 s^{-1} for Aβ_{1-40} fibrils at pH 7.0 and 28 °C.[55] The data analysis described by Sanchez et al. assumes a fibril structure with only one Aβ_{1-40} molecule per 0.48 nm repeat. With two or three molecules per repeat, their analysis would imply k_s values of roughly 0.6 or 0.9 nm/s, much larger than values in Table 1.

In measurements of the association of radio-labeled Aβ_{1-40} with preformed fibrils, and with an initial concentration of the radio-labeled peptide equal to 100 pM in phosphate-buffered saline at room temperature, Esler et al. observed a biphasic association process.[29] Subsequent dissociation rates were also found to be biphasic and to depend on the association time. Similar behavior was observed for association/dissociation with amyloid in brain tissue. These observations led to the proposal of a "dock−lock" mechanism for fibril growth, in which monomers bound to the ends of fibrils are initially in a "docked" state that is in dynamic equilibrium with soluble monomers and slowly convert to a more tightly bound "locked" state. In principle, the dock−lock mechanism can be described by eq 2 above. However, quantitative aspects of the results reported by Esler et al. appear to be inconsistent with our own results. In particular, at 100 pM soluble Aβ_{1-40} concentration, the time scale for adding one molecule to a fibril would be ∼100 h according to k_e values in Table 1 (assuming $k_s = 0$), whereas the "locked" state develops within ∼1 h in the experiments of Esler et al. In addition, under our experimental conditions, $M_{QE} \gg 100$ pM, so that fibrils would shrink rather than elongate.

■ CONCLUSION

Results described above for two Aβ_{1-40} fibril polymorphs demonstrate the efficacy of AFM as a means of quantifying polymorph-specific fibril elongation and shrinkage kinetics and quasi-equilibrium solubilities. The same methods can be applied to other amyloid-forming peptides and proteins. At 24 °C, pH 7.4, and low ionic strength, $\mathcal{A}$ fibrils have greater elongation and shrinkage rates than $\mathcal{Q}$ fibrils but similar solubilities (∼0.4 μM). Solid-state NMR spectra show that a mixture of $\mathcal{A}$ and $\mathcal{Q}$ fibrils evolves toward pure $\mathcal{A}$ fibrils over a period of more than 35 days, indicating that $\mathcal{A}$ fibrils have greater thermodynamic stability under these conditions. At 37 °C, elongation rates are increased, and solubilities are reduced to about 0.06 μM for both polymorphs. Analysis of fibril length distributions during elongation suggests that growth is intermittent, with individual fibrils switching randomly between "on" and "off" states on the 10−70 s time scale. Finally, $\mathcal{A}$ fibrils are significantly more susceptible than $\mathcal{Q}$ fibrils to fragmentation by shear forces, a fact that contributes to the predominance of $\mathcal{A}$ fibrils when Aβ_{1-40} fibrils are grown de novo in agitated solutions.

■ ASSOCIATED CONTENT

Supporting Information

Diagram of dialysis apparatus (Figure S1), TEM images of parent $\mathcal{Q}$ and $\mathcal{A}$ fibrils which were used as seeds (Figure S2), additional representative AFM images from fibril elongation experiments (Figure S3), experimental and simulated histograms of fibril length distributions at 24 °C (Figure S4), dialysis control results and analytical HPLC traces to measure $M_{QE,UV}$ values (Figure S5), experimental and simulated histograms of fibril length distributions at 37 °C (Figure S6), contour plots of fits between experimental and simulated fibril length distributions at 37 °C (Figure S7), and AFM images from fibril fragmentation experiments (Figure S8). This material is available free of charge via the Internet at http://pubs.acs.org.

■ AUTHOR INFORMATION

Corresponding Author

robertty@mail.nih.gov

Present Address

[#]Medical Scientist Training Program, School of Medicine, University of California, San Francisco, California 94143, United States.

Notes

The authors declare no competing financial interest.

■ ACKNOWLEDGMENTS

This work was supported by the Intramural Research Program of the National Institute of Diabetes and Digestive and Kidney Diseases of the National Institutes of Health. We thank Dr. Wai-Ming Yau for synthesizing and purifying $A\beta_{1\text{-}40}$.

■ REFERENCES

(1) Petkova, A. T.; Buntkowsky, G.; Dyda, F.; Leapman, R. D.; Yau, W. M.; Tycko, R. *J. Mol. Biol.* **2004**, *335*, 247.
(2) Petkova, A. T.; Leapman, R. D.; Guo, Z. H.; Yau, W. M.; Mattson, M. P.; Tycko, R. *Science* **2005**, *307*, 262.
(3) Petkova, A. T.; Yau, W. M.; Tycko, R. *Biochemistry* **2006**, *45*, 498.
(4) Paravastu, A. K.; Leapman, R. D.; Yau, W. M.; Tycko, R. *Proc. Natl. Acad. Sci. U.S.A.* **2008**, *105*, 18349.
(5) Goldsbury, C. S.; Wirtz, S.; Muller, S. A.; Sunderji, S.; Wicki, P.; Aebi, U.; Frey, P. *J. Struct. Biol.* **2000**, *130*, 217.
(6) Goldsbury, C.; Frey, P.; Olivieri, V.; Aebi, U.; Muller, S. A. *J. Mol. Biol.* **2005**, *352*, 282.
(7) Kodali, R.; Williams, A. D.; Chemuru, S.; Wetzel, R. *J. Mol. Biol.* **2010**, *401*, 503.
(8) Bertini, I.; Gonnelli, L.; Luchinat, C.; Mao, J. F.; Nesi, A. *J. Am. Chem. Soc.* **2011**, *133*, 16013.
(9) Meinhardt, J.; Sachse, C.; Hortschansky, P.; Grigorieff, N.; Fandrich, M. *J. Mol. Biol.* **2009**, *386*, 869.
(10) Schmidt, M.; Sachse, C.; Richter, W.; Xu, C.; Fandrich, M.; Grigorieff, N. *Proc. Natl. Acad. Sci. U.S.A.* **2009**, *106*, 19813.
(11) del Amo, J. M. L.; Schmidt, M.; Fink, U.; Dasari, M.; Fandrich, M.; Reif, B. *Angew. Chem., Int. Ed.* **2012**, *51*, 6136.
(12) Luhrs, T.; Ritter, C.; Adrian, M.; Riek-Loher, D.; Bohrmann, B.; Doeli, H.; Schubert, D.; Riek, R. *Proc. Natl. Acad. Sci. U.S.A.* **2005**, *102*, 17342.
(13) Parthasarathy, S.; Long, F.; Miller, Y.; Xiao, Y. L.; McElheny, D.; Thurber, K.; Ma, B. Y.; Nussinov, R.; Ishii, Y. *J. Am. Chem. Soc.* **2011**, *133*, 3390.
(14) Scheidt, H. A.; Morgado, I.; Rothemund, S.; Huster, D. *J. Biol. Chem.* **2012**, *287*, 2017.
(15) Sato, T.; Kienlen-Campard, P.; Ahmed, M.; Liu, W.; Li, H. L.; Elliott, J. I.; Aimoto, S.; Constantinescu, S. N.; Octave, J. N.; Smith, S. O. *Biochemistry* **2006**, *45*, 5503.
(16) Torok, M.; Milton, S.; Kayed, R.; Wu, P.; McIntire, T.; Glabe, C. G.; Langen, R. *J. Biol. Chem.* **2002**, *277*, 40810.
(17) McDonald, M.; Box, H.; Bian, W.; Kendall, A.; Tycko, R.; Stubbs, G. *J. Mol. Biol.* **2012**, *423*, 454.
(18) Zhang, R.; Hu, X. Y.; Khant, H.; Ludtke, S. J.; Chiu, W.; Schmid, M. F.; Frieden, C.; Lee, J. M. *Proc. Natl. Acad. Sci. U.S.A.* **2009**, *106*, 4653.
(19) Miller, Y.; Ma, B.; Nussinov, R. *Chem. Rev.* **2010**, *110*, 4820.
(20) Chen, B.; Thurber, K. R.; Shewmaker, F.; Wickner, R. B.; Tycko, R. *Proc. Natl. Acad. Sci. U.S.A.* **2009**, *106*, 14339.
(21) O'Nuallain, B.; Shivaprasad, S.; Kheterpal, I.; Wetzel, R. *Biochemistry* **2005**, *44*, 12709.
(22) Shivaprasad, S.; Wetzel, R. *J. Biol. Chem.* **2006**, *281*, 993.
(23) Williams, A. D.; Shivaprasad, S.; Wetzel, R. *J. Mol. Biol.* **2006**, *357*, 1283.
(24) Komatsu, H.; Feingold-Link, E.; Sharp, K. A.; Rastogi, T.; Axelsen, P. H. *J. Biol. Chem.* **2010**, *285*, 41843.
(25) Sengupta, P.; Garai, K.; Sahoo, B.; Shi, Y.; Callaway, D. J. E.; Maiti, S. *Biochemistry* **2003**, *42*, 10506.
(26) Hasegawa, K.; Ono, K.; Yamada, M.; Naiki, H. *Biochemistry* **2002**, *41*, 13489.
(27) Cannon, M. J.; Williams, A. D.; Wetzel, R.; Myszka, D. G. *Anal. Biochem.* **2004**, *328*, 67.
(28) Kotarek, J. A.; Johnson, K. C.; Moss, M. A. *Anal. Biochem.* **2008**, *378*, 15.
(29) Esler, W. P.; Stimson, E. R.; Jennings, J. M.; Vinters, H. V.; Ghilardi, J. R.; Lee, J. P.; Mantyh, P. W.; Maggio, J. E. *Biochemistry* **2000**, *39*, 6288.
(30) Kellermayer, M. S. Z.; Karsai, A.; Benke, M.; Soos, K.; Penke, B. *Proc. Natl. Acad. Sci. U.S.A.* **2008**, *105*, 141.
(31) Ban, T.; Hoshino, M.; Takahashi, S.; Hamada, D.; Hasegawa, K.; Naiki, H.; Goto, Y. *J. Mol. Biol.* **2004**, *344*, 757.
(32) Ferkinghoff-Borg, J.; Fonslet, J.; Andersen, C. B.; Krishna, S.; Pigolotti, S.; Yagi, H.; Goto, Y.; Otzen, D.; Jensen, M. H. *Phys. Rev. E* **2010**, *82*, 010901.
(33) Schneider, C. A.; Rasband, W. S.; Eliceiri, K. W. *Nat. Methods* **2012**, *9*, 671.
(34) Harper, J. D.; Lieber, C. M.; Lansbury, P. T. *Chem. Biol.* **1997**, *4*, 951.
(35) Harper, J. D.; Wong, S. S.; Lieber, C. M.; Lansbury, P. T. *Chem. Biol.* **1997**, *4*, 119.
(36) Stine, W. B.; Snyder, S. W.; Ladror, U. S.; Wade, W. S.; Miller, M. F.; Perun, T. J.; Holzman, T. F.; Krafft, G. A. *J. Protein Chem.* **1996**, *15*, 193.
(37) Kowalewski, T.; Holtzman, D. M. *Proc. Natl. Acad. Sci. U.S.A.* **1999**, *96*, 3688.
(38) Nichols, M. R.; Moss, M. A.; Reed, D. K.; Lin, W. L.; Mukhopadhyay, R.; Hoh, J. H.; Rosenberry, T. L. *Biochemistry* **2002**, *41*, 6115.
(39) Collins, S. R.; Douglass, A.; Vale, R. D.; Weissman, J. S. *PLoS Biol.* **2004**, *2*, 1582.
(40) Knowles, T. P. J.; Waudby, C. A.; Devlin, G. L.; Cohen, S. I. A.; Aguzzi, A.; Vendruscolo, M.; Terentjev, E. M.; Welland, M. E.; Dobson, C. M. *Science* **2009**, *326*, 1533.
(41) Halverson, K.; Fraser, P. E.; Kirschner, D. A.; Lansbury, P. T. *Biochemistry* **1990**, *29*, 2639.
(42) Hilbich, C.; Kisterswoike, B.; Reed, J.; Masters, C. L.; Beyreuther, K. *J. Mol. Biol.* **1991**, *218*, 149.
(43) Hilbich, C.; Kisterswoike, B.; Reed, J.; Masters, C. L.; Beyreuther, K. *J. Mol. Biol.* **1992**, *228*, 460.
(44) Antzutkin, O. N.; Balbach, J. J.; Leapman, R. D.; Rizzo, N. W.; Reed, J.; Tycko, R. *Proc. Natl. Acad. Sci. U.S.A.* **2000**, *97*, 13045.
(45) Wang, J.; Dickson, D. W.; Trojanowski, J. Q.; Lee, V. M. Y. *Exp. Neurol.* **1999**, *158*, 328.
(46) Tseng, B. P.; Esler, W. P.; Clish, C. B.; Stimson, E. R.; Ghilardi, J. R.; Vinters, H. V.; Mantyh, P. W.; Lee, J. P.; Maggio, J. E. *Biochemistry* **1999**, *38*, 10424.
(47) Zhou, G. Q.; Zhong, W. Z. *Eur. J. Biochem.* **1982**, *128*, 383.

(48) Nguyen, P. H.; Li, M. S.; Stock, G.; Straub, J. E.; Thirumalai, D. *Proc. Natl. Acad. Sci. U.S.A.* **2007**, *104*, 111.
(49) O'Brien, E. P.; Okamoto, Y.; Straub, J. E.; Brooks, B. R.; Thirumalai, D. *J. Phys. Chem. B* **2009**, *113*, 14421.
(50) Takeda, T.; Klimov, D. K. *Biophys. J.* **2009**, *96*, 4428.
(51) Creighton, T. E. *Proteins: Structures and Molecular Properties*; 2nd ed.; W.H. Freeman: New York, 1992.
(52) O'Nuallain, B.; Wetzel, R. *Proc. Natl. Acad. Sci. U.S.A.* **2002**, *99*, 1485.
(53) Tjernberg, L. O.; Pramanik, A.; Bjorling, S.; Thyberg, P.; Thyberg, J.; Nordstedt, C.; Berndt, K. D.; Terenius, L.; Rigler, R. *Chem. Biol.* **1999**, *6*, 53.
(54) Lomakin, A.; Chung, D. S.; Benedek, G. B.; Kirschner, D. A.; Teplow, D. B. *Proc. Natl. Acad. Sci. U.S.A.* **1996**, *93*, 1125.
(55) Sanchez, L.; Madurga, S.; Pukala, T.; Vilaseca, M.; Lopez-Iglesias, C.; Robinson, C. V.; Giralt, E.; Carulla, N. *J. Am. Chem. Soc.* **2011**, *133*, 6505.